ACSNANO

www.acsnano.org

Ultrafast and Controllable Phase Evolution by Flash Joule Heating

Weiyin Chen, John Tianci Li, Zhe Wang, Wala A. Algozeeb, Duy Xuan Luong, Carter Kittrell, Emily A. McHugh, Paul A. Advincula, Kevin M. Wyss, Jacob L. Beckham, Michael G. Stanford, Bo Jiang, and James M. Tour*

Cite This: *ACS Nano* 2021, 15, 11158−11167

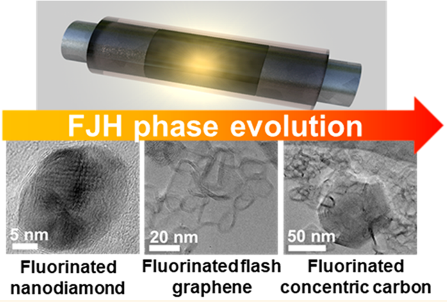

ABSTRACT: **Flash Joule heating (FJH), an advanced material synthesis technique, has been used for the production of high-quality carbon materials. Direct current discharge through the precursors by large capacitors has successfully converted carbon-based starting materials into bulk quantities of turbostratic graphene by the FJH process. However, the formation of other carbon allotropes, such as nanodiamonds and concentric carbon materials, as well as the covalent functionalization of different carbon allotropes by the FJH process, remains challenging. Here, we report the solvent-free FJH synthesis of three different fluorinated carbon allotropes: fluorinated nanodiamonds, fluorinated turbostratic graphene, and fluorinated concentric carbon. This is done by millisecond flashing of organic fluorine compounds and fluoride precursors. Spectroscopic analysis confirms the modification of the electronic states and the existence of various short-range and long-range orders in the different fluorinated carbon allotropes. The flash-time-dependent relationship is further demonstrated to control the phase evolution and product compositions.**

KEYWORDS: *flash Joule heating, carbon materials, flash graphene, fluorinated carbon allotropes, nanodiamond, concentric carbon*

INTRODUCTION

The short-range order of adjacent carbon atoms in materials determines their interatomic bonding and hybridization states, which produce distinctive physical, chemical, and electronic properties.[1−5] For example, graphene, with its two-dimensional (2D) sheet-like structure, is composed of sp^2-hybridized carbon in a hexagonal honeycomb lattice unit and it has zero band gap, with high in-plane carrier mobility, thermal conductivity, and mechanical strength.[6,7] In contrast, diamond is a three-dimensional (3D) material with sp^3-hybridized carbon that exhibits a large band gap (>3 eV), characteristic fluorescence, and bio-compatibility.[2,8] Therefore, the selective synthesis of different allotropes using controllable phase transformation is of great importance for researchers to exploit materials to produce advanced properties for different applications.[9] Furthermore, theoretical simulations have shown small formation energy differences between diamond and graphene (0.01−0.04 eV/atom).[10] The large activation energy (≥0.4 eV/atom)[10] required to weaken the C═C or C−C bonds and to rearrange the short-range order of the adjacent carbon atoms makes it challenging to synthesize the desired carbon allotropes from a single precursor. As a consequence, external extreme conditions, such as high temperature and high pressure (HTHP, >1000 °C, >1 GPa), are usually required to synthesize diamonds from carbonaceous materials with sp^2-hybridized carbon atoms,[11−13] while high temperature (>1000 °C) is needed to prepare onion-like carbons (OLC) or carbon nanotubes with high crystallinity from diamond-like carbons.[11,14,15]

Several recent reports have shown that transit of reaction materials through intermediate states, such as the carbon liquid phase[11,12] or isolated carbonaceous radicals (C_2, C_3, C_2H_2, and other radicals),[16] had significant consequences for the subsequent formation of various solid nanocarbon products. The intermediate states, which are produced by femtosecond laser pumping[12] or by a plasma source[17] with high energy densities, are inherently transient with high reactivities and short time scales. The phase transition kinetics of these intermediate states were studied based on the cooling-adiabat process, and different carbon allotropes, such as nanodiamonds (NDs, sp^3-hybridized carbon) and OLCs (sp^2-hybridized

Received: April 26, 2021
Accepted: June 10, 2021
Published: June 17, 2021

https://doi.org/10.1021/acsnano.1c03536

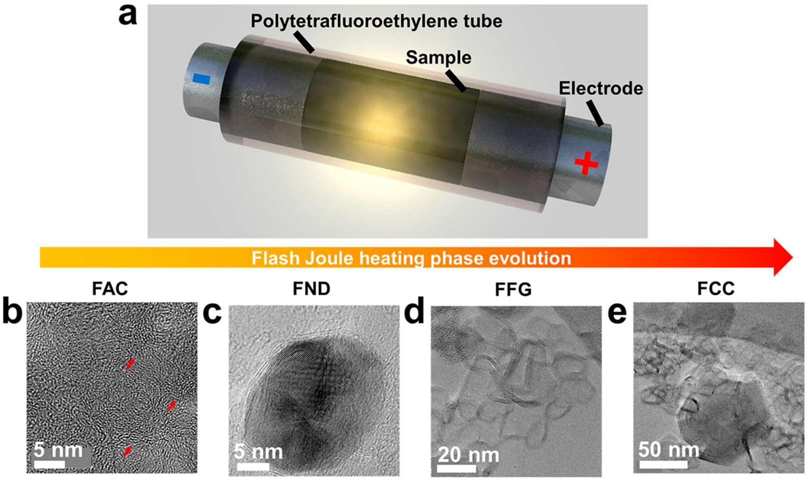

Figure 1. Phase evolution of carbon materials. (a) Schematic diagram of FJH setup to study phase evolution. (b−e) HR-TEM images show the specific phases of carbon materials at different flash stages. (b) FAC; (c) FNDs; (d) FFG; and (e) FCC products.

carbon), have been observed as final solid products. Conversely, atomistic simulations and experiments have confirmed one of the most effective phase transition pathways is in the control of the interlayer C−C bonds.[1,10,18] The formation of NDs could be induced by fluorination[2,18] or nano-indentation treatment[1] from AB-stacked bilayer graphene, which indicates the important roles of interatomic distance and interlayer C−C bonds in phase transformation. Direct ion beam or electron beam bombardment could “unzip” the diamond structure along the [111] direction and trigger the formation of graphene at room temperature.[10]

The precursor types and structures, along with the reaction conditions, have been confirmed to have strong effects on the final structures. It is reported that laser-assisted fluorinated diamond and fluorinated graphene synthesis from Teflon can be achieved using a CO_2 infrared pulsed laser under ambient pressure by varying the defocus values,[2] during which the transient temperature can be as high as 2300 K within milliseconds.[19] Since there is some overlap between the laser wavelength and the shoulder of the C-F stretching peaks in the fluoropolymers, the photon absorption occurs and the photothermal/photochemical effects induce the formation of the FND.[2] While starting from commercial polyimide films,[6] woods,[20] or other natural sources, like coals,[21] laser-induced graphene with different degrees of graphitization and distinct morphology features can be prepared. The content of fluorine in the sample has been confirmed to play an important role in the stabilization of sp^3-hybridized carbon and the formation of interlayer C−C bonds. While the detonation method provides the transient high pressure and high temperature, the NDs become more thermodynamically stable than graphite under these conditions as shown in the phase diagram.[11] Thus, the NDs form in the detonation method. In this work, we further demonstrate the formation of different fluorinated carbon allotropes from various types of organic fluorine compounds and fluoride precursors by the flash Joule heating (FJH) method. FJH is an electrothermal approach that has the potential to reach more than 3100 K within milliseconds.[22−27] Spectroscopic analysis confirms the modification of the electronic states and the existence of various short-range and long-range orders in different fluorinated carbon allotropes. We further explore the flash time-dependent relationship on products, which demonstrates the ultrafast and controllable phase evolution during the FJH process. The flash conditions for the formation of fluorinated nanodiamonds (FND), fluorinated turbostratic graphene (FTG), and fluorinated concentric carbon (FCC) material are provided for seven different types of organic fluorine compounds and fluoride precursors. FJH offers rapid access to different carbon allotropes and has the potential for production of functionalized carbon materials without the need for solvents or any wet methods, making them potentially more attractive for scaling.

RESULTS AND DISCUSSION

Figure 1a shows the FJH setup. Different types of reactants were tightly compressed inside a polytetrafluoroethylene (PTFE) tube, and the electrodes were tungsten carbide rods with graphite spacers. The reactants were mixtures of various organic fluorine compounds: PTFE, polyvinylidene fluoride (PVDF), 1,1,1,2,2,3,3,4,4,5,5,6,6,7,7,8,8-heptadecafluoro-10-iododecane, 1*H*,1*H*-perfluoro-1-dodecanol, and NaF. There were intrinsic sp^3-hybridized carbon atoms in the organic fluorine compounds that could lower the formation energies of FND. It has been reported that selective etching of carbides, such as silicon carbide (with intrinsic sp^3-hybridized carbon), can remove the Si atoms from the carbide lattice and induce the direct formation of crystalline diamond-structured carbon.[28] Carbon black (CB) or flash graphene (FG, 20 wt %) was added and homogeneously mixed to obtain the reactants with the desired conductivity. During the FJH process, a large amount of energy from electric heating triggers the formation of various fluorinated carbon allotropes from the different precursors. Additional experimental details and a photo of the FJH setup can be found in the Experimental Section and Figure S1. By using PTFE and CB (20 wt %) as the reactants, the formation of specific phases of carbon materials at different flash stages could be distinguished using microscopic imaging to determine the morphology. By controllably tuning the flash conditions, fluorinated amorphous carbon (FAC), FND (sp^3-carbon), fluorinated flash graphene (FFG, sp^2-carbon), and FCC with high crystallinity and a polyhedral shape can be seen in sequence as shown in Figure 1b−e.

High resolution transmission electron microscopy (HR-TEM) was conducted to identify the atomic structure of the different carbon allotropes in Figure 2. As shown in Figure 2a,

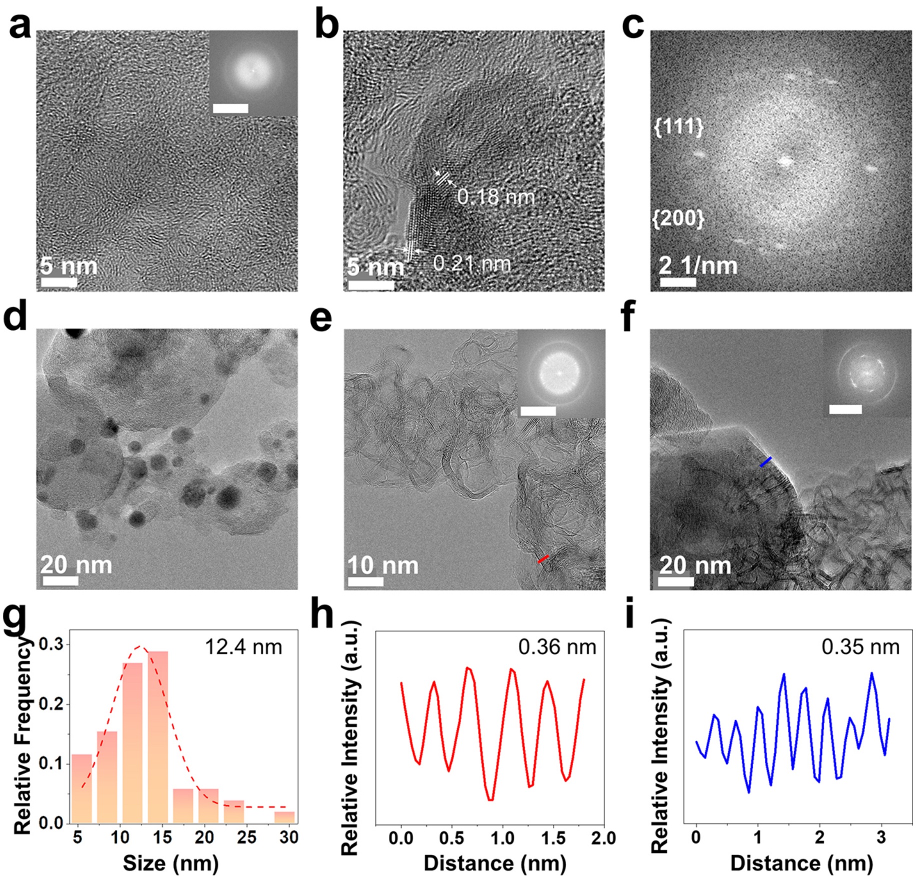

Figure 2. Microscopic analysis of carbon materials at different stages of phase evolution. (a) HR-TEM image of FAC. The inset is the FFT showing the blurred ring. Scale bar is 5 nm^{-1}. (b) HR-TEM image of FNDs. (c) FFT image of selected area from (b). (d) TEM image shows the distribution of FNDs. (e) TEM image of FFG. The inset is the FFT showing multiple distinct Bragg spots. Scale bar is 5 nm^{-1}. (f) TEM image of FCC with high crystallinity. The inset is the FFT showing the arc fragments with distinct Bragg spots. Scale bar is 5 nm^{-1}. (g) A statistical survey showing the FND sizes, *N* = 50. (h) Line scan showing interlayer spacing of FFG in (e). (i) Line scan showing interlayer spacing of FCC in (f).

the irregular stripes reflect the amorphous nature of the initial product after a short flash pulse. The inset shows the fast Fourier transform (FFT) result reporting the blurred ring, which also indicates the amorphous nature. In contrast, the FNDs (Figure 2b−d) display a facet distance of 0.21 and 0.18 nm, which are the characteristic distances of {111} and {200} diamond cubic, respectively.[29] From the HR-TEM image in Figure 2b, the FND was terminated by the {111} plane, which was the lattice plane with minimal energy compared to other low index planes. The corresponding FFT image in Figure 2c shows the Bragg spots with four-fold symmetry, which was the reflection of the {111} plane.[2] There was more than one set of Bragg spots, indicating different orientations of the FNDs. The {200} plane showed a very weak signal in the FFT image, which was the result of destructive interference in diamond cubic.[28] Figure 2d shows the distribution of FNDs, and the contrasting difference in the TEM images makes it possible to distinguish the FNDs from the FAC substrate. The average size of the FND is 12.4 nm as shown in Figure 2g (the number of samples *N* = 50), and the largest FND as shown in Figure 1c is ∼40 nm with high crystallinity. Figure 2e shows the TEM image of another typical carbon allotrope, FFG. The inset shows the FFT, indicating multiple distinct Bragg spots, which reflect the misorientation among different graphene sheets in the [002] stacking direction and confirm the turbostratic feature of the FFG.[22,30] The average size of the FFG was ∼20 nm, which is similar to the unfunctionalized FG derived from CB.[26] The intensity profile (red line scan as shown in Figure 2e) reports that the average interlayer spacing of FFG was 0.36 nm (Figure 2h), which was ∼7% larger than commercial graphite (0.33 nm) that was composed of AB-stacking graphene layers, indicating weaker coupling interaction between adjacent layers.[26] Longer flash duration induced the formation of FCC with a polyhedral structure and high crystallinity as shown in Figure 2f. HR-TEM images demonstrate that graphene sheets with gradually changed sizes shared a common center, while the periphery of the FCC had a higher degree of crystallinity than the center region. In the center region, the existence of an amorphous region and grain boundaries could be observed. Theoretical analysis has confirmed a higher graphitization degree at peripheral sections due to the surface tension resulting from the nanometer-sized curvature of carbon nanomaterials.[31] The inset in Figure 2f shows the FFT image indicating the arc fragments with bright and distinct Bragg spots, which reflects that there are graphene layers with different orientations in the *c* axis and the coexistence of both AB stacking graphene and turbostratic graphene. The intensity profile (blue line scan as shown in Figure 2f) shows the average interlayer spacing of CC was 0.35 nm (Figure 2i), which reflects a common interlayer expansion induced by a bent structure.

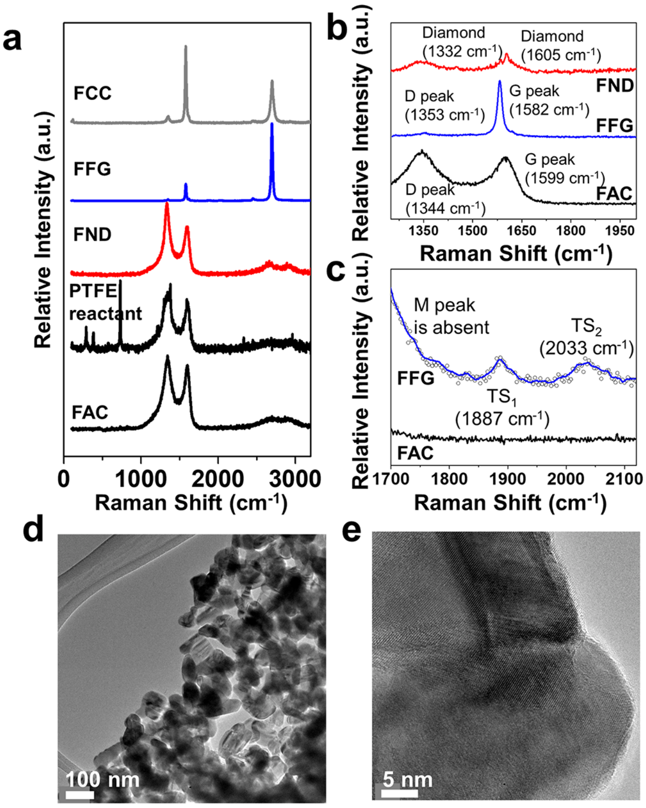

Figure 3. Spectroscopic analysis of carbon materials at different stages of phase evolution. (a) Raman spectra of FAC, PTFE reactant, FND, FFG, and FCC. (b) High resolution Raman spectra showing specific peaks for FFG and FND. (c) High resolution Raman spectra showing the TS series peaks of turbostratic FFG. (d, e) TEM images of FND sample after TGA treatment.

To further distinguish between different carbon allotropes, Raman spectroscopy was conducted, since various allotropes have distinct phonon modes.[14,32,33] As shown in Figure 3a,b, for FAC, two obvious peaks, a D peak at 1344 cm^{-1} (breathing mode of sp^2-carbon atoms in rings) and a G peak at 1599 cm^{-1} (bonds stretching of all pairs of sp^2-carbon atoms in rings and chains) and the absence of a 2D peak (second order zone-boundary phonons in graphene) indicate the amorphous nature of FAC.[32] Sharp peaks at ∼730 and 1380 cm^{-1} indicate the existence of PTFE in the PTFE reactant mixture. After the flash reaction, the characteristic FND region shows a red shift of the D peak from 1344 to 1333 cm^{-1} and the increasing ratio of the D peak to the G peak (I_D/I_G) from 1.08 to 1.52, which indicates the introduction of the electron-withdrawing F substituents and the breaking of the periodic sp^2-carbon network structure. In contrast, the characteristic FFG region shows a weak D band and a high ratio of I_{2D}/I_G with a value >4.6, which indicates a low defect density and high quality turbostratic graphene.[26] Compared to the D and G peaks in graphitic materials, such as FFG and FAC, there were two diamond peaks at 1332 and 1605 cm^{-1} in the FND sample after the thermal purification treatment,[2,17] as shown in Figure 3b. The thermal gravimetric analysis (TGA) curve of the FND sample is shown in Figure S2. The corresponding TEM images of a thermally purified FND sample can be seen in Figures 3d,e and S3. The isolated FNDs can be seen, with no obvious amorphous carbon at the boundary of the FNDs. This confirmed that thermal treatment is an effective method to purify the flash product. A ridge-like structure, the grain boundary, can be seen in Figure 3e and Figure S3, which indicates high crystallinity of the FNDs. Compared to the reactant PTFE, the flash product had higher dispersibility as shown in Figure S4; this product has the potential to be used as a lubricant additive.[22,30] Since the Raman tensor for the sp^3-carbon structure causes a narrower Raman cross section compared to a conjugated sp^2-carbon structure, the intensities of the D and G peaks are much higher than diamond Raman peaks in the spectra.[32] The characteristic TS$_1$ (1887 cm^{-1}) and TS$_2$ (2033 cm^{-1}) peaks and the absence of an M peak (1750 cm^{-1}) indicate the turbostratic nature of the FFG as shown in Figure 3c.[22] The FAC sample was used as a comparison. Since there was no regular stacking sequence along the *c* axis in FAC, neither the M peak nor the TS series peaks (TS$_1$ and TS$_2$) can be seen in the spectrum. The TGA curve in Figure S5 shows a higher thermal stability of the crystalline FFG than amorphous FAC. The purity of FFG can reach >90% since there is only one stage of the mass loss. The conclusion is consistent with the TEM images as shown in Figures 1 and 2. FNDs are embedded in the amorphous carbon substrate, and the purity of FNDs is at least 30% (Figure S2). TEM images of the FND sample after TGA treatment show the removal of the amorphous carbon substrate and the existence of the NDs. The estimated product yield is calculated as the ratio between the mass of product after thermal purification treatment and mass of the reactant. TGA curves of FND and FFG samples indicate the yields are ∼15% and ∼40%, respectively, as shown in Figures S2 and S5. Longer flash duration induces the formation of the FCC with I_{2D}/I_G ∼ 0.55. There are no obvious TS series peaks or M peak as shown in Figure S6, which indicates there might be some sub-stacking sequence along the *c* axis rather than AB (Bernal) stacking or random stacking. The peak positions of G and 2D peaks were 1580 and 2701 cm^{-1}, respectively, and there was no obvious downshift compared to graphene sheets, which excluded the existence of a fullerene shell in the FCC polyhedral structure.[34] The X-ray diffraction (XRD) results in Figure S7 further comfirm the existence of the nanodiamonds in FND samples,[17] the turbostratic nature of the graphene in FFG samples,[22] and the long-order staking along the Z axis in FCC samples.[22,26]

X-ray photoelectron spectroscopy (XPS) was also conducted to analyze the elemental content and chemical bonds in the various carbon allotropes.[35] Survey spectra in Figure 4a reveal that only C and F exist in the samples, which excludes interference from other elements, such as Cu that has a similar lattice structure. The atomic ratio of C to F can be calculated based on the integrated area of C 1s and F 1s for elemental analysis. Table S1 lists the element content in the fluoropolymers and different carbon allotropes. The F:C in PTFE was 2.03, whereas the ratio in FND was 0.25 and in FFG it was ∼0.08, which indicate the important role of fluorine in the formation of different carbon allotropes. The chemical structures of FND and FFG were determined by high resolution F 1s and C 1s XPS spectra. The covalent $-CF_2$ at 292.5 eV can be found in PTFE and FND as shown in Figure 4b, which recently has been verified to play an important role in forming sp^3-carbon in the carbon materials.[2,18] The peak at 285.2 eV derived from C-C can be found in the FND sample, while, in the FFG sample, the C=C peak at 284.8 eV reflects the graphitic structure. The chemical environment can also be reflected by F 1s spectra as shown in Figure 4c. Both semi-

https://doi.org/10.1021/acsnano.1c03536
ACS Nano 2021, 15, 11158−11167

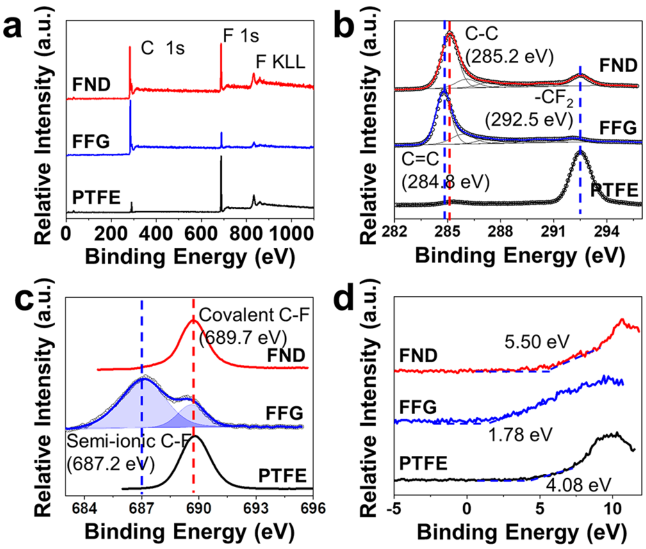

Figure 4. Spectroscopic analysis of carbon materials at different stages of phase evolution. (a) XPS spectra of FND, FFG, and PTFE. (b, c) High resolution C 1s and F 1s spectra of FND, FFG, and PTFE. (d) Valence band XPS spectra of FND, FFG, and PTFE.

Table 1. Effect of Flash Reactant on the Synthesis of Carbon Allotropes

reactant	FND	FFG	FCC
PTFE with CB	yes (~50 nm)	yes	yes
PTFE with FG	yes (~40 nm)	yes	yes
PVDF with CB	no	yes	yes
1,1,1,2,2,3,3,4,4,5,5,6,6,7,7,8,8-heptadecafluoro-10-iododecane with CB	yes (~60 nm)	yes	yes
1*H*,1*H*-perfluoro-1-dodecanol with CB	yes (~80 nm)	yes	yes
PTFE with CB and NaF	yes (<10 nm)	no	no
CB	no	yes	yes[24]

ionic C−F (~687.1 eV) and covalent C−F bonds (~689.7 eV) can be seen in the FFG sample, whereas only covalent C−F bonds can be found in FND and PTFE, which agrees with the result in our previous work using laser formation processes.[2]

The *D* parameter measures the binding energy separation between maximum and minimum valence levels in differentiated C KLL Auger transition spectra. In diamond and graphene, the values are 13 and 21 eV, respectively.[22] The larger *D* parameter generally infers a higher sp^2:sp^3 ratio. The C KLL and corresponding differentiated spectra are reported in Figures S8−S10, and the *D* parameters are listed in Table S2. Those products with periodic graphitized structures, such as FG, FFG, and FCC, had *D* parameters close to 21 eV, and the organic fluorine compounds, like PVDF and PTFE, had the values close to 13 eV, which indicate the sp^3-carbon atoms dominate. The FND had a *D* parameter of 16.0 eV, which indicated the existence of both sp^3-carbon atoms and sp^2-carbon atoms, which result from a mixture of the FND and amorphous carbon as shown in HR-TEM images. The band gaps of samples were further determined by valence band XPS (VB-XPS), which is a powerful method to measure the energy difference (E_g) between the conduction band minimum (CBM) and valence band (VB). As shown in Figure 4d and Table S2, the band gaps of FND, FFG, and PTFE are 5.50, 1.78, and 4.08 eV, respectively. The large band gap in the FND sample indicates the insulating feature of the FND. E_g for FFG is between 0 and 3 eV, which infers that it is a typical semiconductor and might result from the formation of semi-ionic C−F and covalent C−F bonds.

To further explore the effect of flash reactants on phase evolution of carbon materials, seven different combinations of organic fluorine compounds and fluorides were used: (1) CB; (2) PTFE and CB; (3) PTFE and FG; (4) PVDF and CB; (5) PTFE, CB, and NaF, (6) 1,1,1,2,2,3,3,4,4,5,5,6,6,7,7,8,8-heptadecafluoro-10-iododecane and CB, (7) 1*H*,1*H*-perfluoro-1-dodecanol and CB. The results are listed in Table 1 based on the microscopic and spectroscopic analysis as shown in Figures S11−S19. Accordingly, this would probably be a good method for the destruction and upcycling of per- and polyfluoroalkyl substances (PFAS), and this is currently under exploration in our laboratory.

Figure S11 shows TEM images of flash product made from a blend of PVDF with 20 wt % CB. Figures S12 and S13 show the XPS analysis of PVDF and flash product derived from PVDF with 20 wt % CB, respectively. Compared to PTFE, PVDF has a lower F:C ratio (F:C ratios of PTFE and PVDF were 2.03 and 0.98 from the XPS result). As a consequence, there was no FND formed, which indicates the F was important for the formation and stability of FND when compared to other carbon allotropes. Only FCC with a polyhedral structure could form as the final product, which indicates that FCC was the most stable allotrope under these conditions. The crystallinity of the conductive additives might also play an important role in the formation of different carbon allotropes, since the crystalline additives could act as the seeds for the nucleation, which bypasses the potential energy during heterogeneous nucleation.[36] Hence, CB was substituted by FG derived from CB.[26] The TEM images of the crystalline FG derived from CB are shown in Figure S14. However, there was no obvious difference for the formation of different carbon allotropes. As shown in Figure S15, the formation of FNDs, which were embedded in the amorphous carbon substrate, could be seen. This indicated that the nucleation of FNDs began from the PTFE instead of crystalline FG, since the lattice parameters for sp^2-carbon and sp^3-carbon skeletons are distinct.[37] A previous report has shown that small NDs or metal carbides could be used as seeds to grow larger diamonds,[28] which indicated lattice matching was important for the seed candidates. Increasing the fluorine ratio by adding extra fluoride, such as NaF, was also explored as shown in Figures S16 and S17. Many FNDs with the size <10 nm can be seen, while the addition of NaF facilitated the etching effect toward the carbon materials during the flash reaction. As a consequence, some large holes >50 nm can be seen in Figure S16. The other organic fluorine compounds, such as 1,1,1,2,2,3,3,4,4,5,5,6,6,7,7,8,8-heptadecafluoro-10-iododecane and 1*H*,1*H*-perfluoro-1-dodecanol, can also be starting materials for the formation of the FNDs. As shown in TEM images (Figures S18 and S19), the size of NDs can reach ~80 nm.

The effect of the flash duration on phase evolution of carbon materials was explored. The changing of flash duration will alter the total electrothermal energy that is put into the system, which directly determines the reaction process and final products. Here, PTFE with 20 wt % CB was used as the

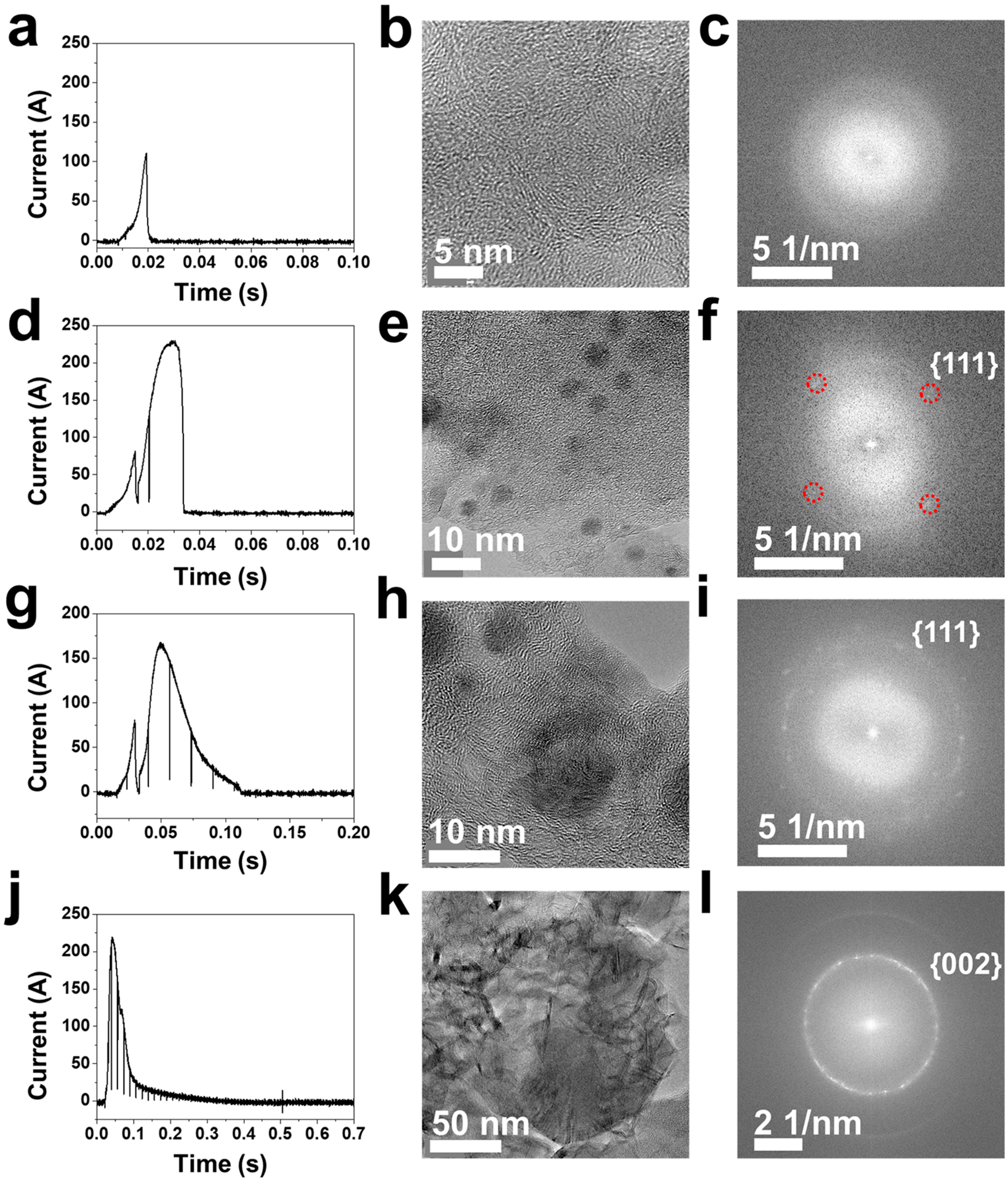

Figure 5. Effect of flash duration on phase evolution of carbon materials. (a, d, g, j) Currents recorded through the carbon sources during different flash durations of 10, 35, 100, and 500 ms, respectively. (b, e, h, k) The HR-TEM images of the carbon materials at corresponding different stages in the same row. (c, f, i, l) Corresponding FFT images of the HR-TEM images in the same row.

reactant. As shown in Figure 5a−c, a very short flash duration (∼10 ms) was used, and the current was to >100 A at this first stage. The TEM image indicated that only FAC was present, and the FFT showed a blurred ring, an indication of amorphous features. The current reached its highest value of 200−230 A after ∼35 ms as shown in Figure 5d. Small FNDs started to form and they were embedded in the amorphous carbon substrate as shown in Figure 5e,f. Figure S20 shows that the average size of the FND particles was 4.06 ± 1.22 nm (N = 100) at the second stage. With a further increase in the flash duration to >100 ms, the I−t curve showed the current started to decrease to 10−20 A as shown in Figure 5g. In this case, the size of ND continued to increase (Figure 5h) and NDs up to 40 nm can be seen in Figure 1c; there was some graphene shell formation on the surface. The end of the power-law decrease of the current was at ∼500 ms as shown in Figure 5j. The FCC structure is identified in the TEM image with the size reaching several hundred nanometers. There were many FFG sheets around the large FCC, which has been shown to merge with CC to increase the size of the CC structure.[26]

The mechanism for the formation of different carbon allotropes is proposed in Figure 6. Relay-controlled discharge through the reactant powder results in rapid heating of the mixture to ∼3000 K within several ms, and the reactant powder experiences ultrafast cooling with the average as fast as ∼10^4 K s^{-1}.[22] During the flash duration, the fluoropolymer is rapidly heated and forms FND particles, while FAC is graphitized and forms FFG. A longer flash duration can further trigger the surface graphitization of the FND particles, and these particles are converted into FCC with a highly graphitized structure and polyhedral shape as shown in Figure 6a−c. During the discharge duration, the C−F bonds in the fluoropolymer are broken, and a F-containing gas phase, such as HF, can form. This process will result in the generation of

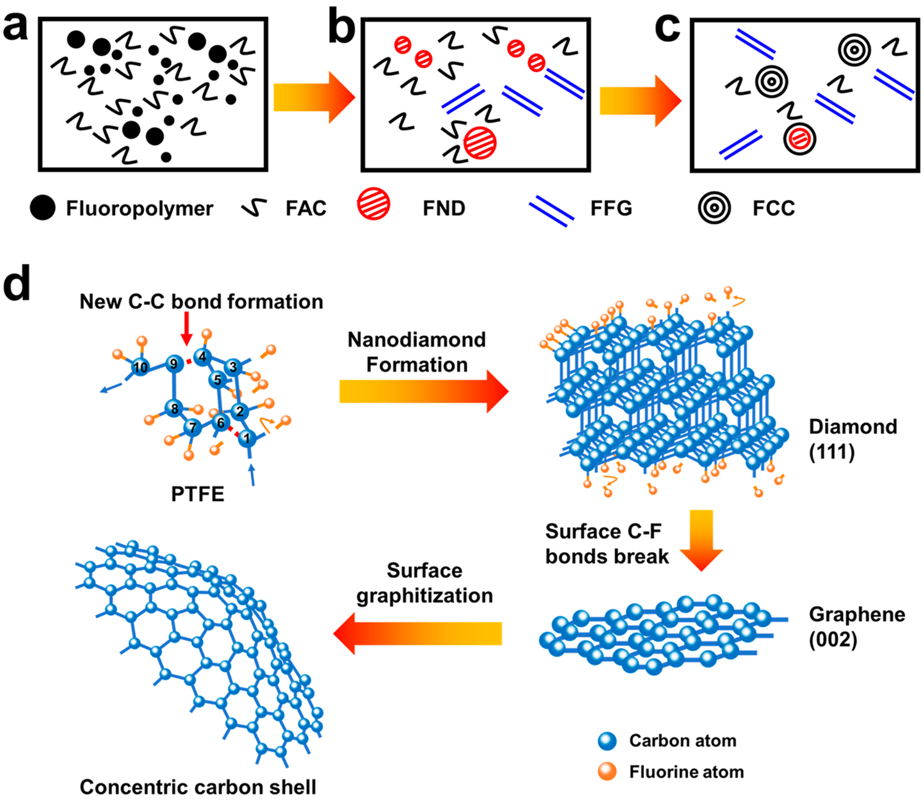

Figure 6. Proposed mechanism for the phase evolution of fluorinated flash nanocarbons. (a−c) Schematic representing the flash product mixtures formed during different stages of the FJH process. (a) Initially, at low energy inputs, a combination of fluoropolymer and FAC is observed. (b) Subsequently, upon increasing the energy input, FND formation ensues, and some of the FAC is converted into FFG. (c) After further addition of energy, the FNDs in the product mixture become converted into FCC, and more of the FAC becomes converted into FFG. (d) Schematic of the proposed mechanism for a single particle undergoing the formation of FND from PTFE, followed by subsequent conversion of the FND into polyhedral FCC. The conversion from FND to FCC begins at the surface of the FND and progresses toward the center of the FND particle.

C−C bonds (red dashed line shown in Figure 6d) and formation of the carbon skeleton, followed by the growth of FND particles. In the flash reaction, the fluorination of the carbon species is vital for the formation of FNDs. Since the difference of electronegativities between C and F is 2.43, covalent C−F bonds are strongly polarized toward the F atoms and the electron density near the C atoms decreases. By forming the sp^3-hybridized C atoms and additional C−C bonds, the paired electrons are shared by these C atoms that are electron deficient and the system energy is lower. Previous simulation has shown that the formation energy of the fluorinated graphene (C_2F configuration) is lower with extra interlayer C−C bonds.[18] These results can be used to explain the formation of the FNDs in the flash products when starting from highly fluorinated reactants, such as PTFE, 1,1,1,2,2,3,3,4,4,5,5,6,6,7,7,8,8-heptadecafluoro-10-iododecane, and 1*H*,1*H*-perfluoro-1-dodecanol. When starting from PVDF, there is no FND formation, and in the flash product, the fluorine content is only ∼0.9%, which is much lower than the fluorine content in the FND sample by using PTFE as the reactant. The loss of fluorine can be attributed to the production of HF gas during the flash process. Because the H−F bond is exceptionally energetically strong, and C−H bonds have lower bond dissociation energies than C−F bonds, decomposition with loss of HF, leading to the formation of carbon species with low fluorine content, is far more favorable for PVDF than for the other starting materials that were tried as reactants here. Increasing the flash duration graphitizes the FND particles from the surface.[15,31] The longer duration further breaks C−F bonds at the surface of FND particles and induces the formation of the (002) plane in graphene from the {111} planes in the FND particles. The fragments of the graphitized region on the surface can merge and form the FCC shells with a polyhedral shape at the outer surface.[14] The progress of graphitization moves to the interior of the FND particles, and the FND particles are converted into FCC with a highly graphitized structure and polyhedral shape as shown in Figure 6d. TEM images in Figure S21 show some FND enclosed by graphene shells, which is the intermediate stage before the full graphitization of the FNDs.

CONCLUSIONS

In summary, different fluorinated carbon allotropes such as FFG, FNDs, and FCC are synthesized in <1 s by tuning the flash conditions, which is effective, fast, and affordable. Spectroscopic analysis confirms the modification of the electronic states by fluorination and the existence of various short-range and long-range orders in different fluorinated carbon allotropes. Our work further expands the FJH-directed synthesis for the production of various carbon allotropes other than intrinsic FG, which broadens the applications for phase selective syntheses using the FJH process. The FJH process is especially useful to generate metastable phases that are difficult to synthesize by conventional methods such as chemical vapor deposition or hydrothermal methods.

Table 2. Flash Parameters for Different Reactants (Categories 1−7)[a]

	1	2	3	4	5	6	7
reactant	CB	PTFE + CB (20 wt %)	PTFE + FG (20 wt %)	PVDF + CB (20 wt %)	PTFE + CB (20 wt %) + NaF (10 wt %)	A[b] + CB (20 wt %)	B[c] + CB (20 wt %)
sample mass	30 mg	40 mg	40 mg	40 mg	40 mg	40 mg	40 mg
sample resistance	∼0.7 Ω	∼1.5 Ω	∼1.5 Ω	∼1.5 Ω	∼3.5 Ω	∼0.5 Ω	∼1.0 Ω
discharge voltage	110 V	120−150 V					
flash duration	10−500 ms						
total capacitance	60 mF						
chamber atmosphere	Ar or N_2 (∼1 atm)						

[a] To simplify the table, symbols are used to refer to different reactants. [b] A: 1,1,1,2,2,3,3,4,4,5,5,6,6,7,7,8,8-heptadecafluoro-10-iodododecane. [c] B: 1*H*,1*H*-perfluoro-1-dodecanol.

METHODS/EXPERIMENTAL SECTION

Materials. Carbon black (CB, APS 10 nm, Black Pearls 2000) was purchased from Cabot Corporation. Polytetrafluoroethylene (PTFE, AF2400) powder was purchased from Teflon AF. Polyvinylidene fluoride (PVDF, 121120-80G) powder was purchased from MTI Corp. NaF powder (99+%, A.C.S. reagent, 201154-100G) was purchased from Sigma-Aldrich. 1,1,1,2,2,3,3,4,4,5,5,6,6,7,7,8,8-Heptadecafluoro-10-iodododecane (370525-25G, 96%) was purchased from Sigma-Aldrich. 1*H*,1*H*-Perfluoro-1-dodecanol, tech (423-65-4, 90%), was purchased from Alfa Aesar. Tungsten carbide cylinder rods (4 mm diameter) were used as the electrodes. Polytetrafluoroethylene tubes (ID = 4 mm, length = 6 cm) were used as the FJH reaction vessels.

FJH System. The FJH reaction box, which provides high compression force to the reactants, and the circuit diagram of the FJH setup are shown in Figure S1. A PTFE tube with a thick wall (∼1 cm) was used so as to reduce damage to the tube and to hold high pressures during the FJH reaction and was loaded with various reactants. Graphite spacers and tungsten carbide cylinder rods were used as electrodes to compress the reactants as shown in Figure S1. A gas absorber is used in the exhaust of the FJH system, and the active species is soda lime, which is $Ca(OH)_2$ with 3% NaOH. $Ca(OH)_2$ reacts with HF to form CaF_2. NaOH accelerates the kinetic process of the reaction.[38] In this work, seven different reactants were used to prepare various carbon allotropes. The reactants included a mixture of (1) CB, (2) PTFE and CB, (3) PTFE and CB-derived FG, (4) PVDF and CB, (5) PTFE, CB, and NaF, (6) 1,1,1,2,23,3,4,4,5,5,6,6,7,7,8,8-heptadecafluoro-10-iodododecane and CB, and (7) 1*H*,1*H*-perfluoro-1-dodecanol and CB. The electrical energy was provided by a capacitor bank in the circuit with a total capacitance of 60 mF. The capacitor bank was charged by a d.c. supply that could reach 400 V. The flash duration was controlled by an Arduino controller relay in the circuit acting as a high-speed switch. The reactant resistances for various reactants were different, and the flash conditions were changed to control the total input electrothermal energy. The parameters are listed in Table 2. Unless specified, the mass ratios of CB and NaF were 20% and 10%, respectively, in the reactants (if added). More safety notes and a circuit diagram of the FJH setup are in the Supporting Information and our previous publications.[9,20,24,28] ***Caution!*** *Ensure that all safety precautions are observed to mitigate electrocution. As a last measure, be sure to wear thick rubber gloves that extent to the elbows. After the FJH reaction, it is suggested to allow the apparatus to cool and vent for 3−5 min.*

Characterization. TEM images were taken with a JEOL 2100F field emission gun TEM at 200 kV. XPS data were collected with a PHI Quantera SXM Scanning X-ray Microprobe with a base pressure of 5×10^{-9} Torr. Survey spectra were recorded using 0.5 eV step sizes with a pass energy of 140 eV. Elemental spectra and VB-XPS were recorded using 0.1 eV step sizes with a pass energy of 26 eV. The C KLL spectra (100 scans, 1190−1246 eV) were recorded using 0.4 eV step sizes with a pass energy of 112 eV. The XPS spectra were corrected using the C═C (284.8 eV) as reference. The peak positions of the FNDs and PTFE were corrected by the covalent CF_2 bond at 292.5 eV. Raman spectra were collected with a Renishaw Raman microscope using a 532 nm laser with a power of 5 mW. A 50× lens is used for local Raman spectra. TGA was performed on a Mettler Toledo TGA/DSC 3+ system. TGA and DSC data were collected from 25 to 800 °C under air. The heating rate was set to 10 °C/min from 25 to 400 °C, 1 °C/min from 400 to 700 °C, and 10 °C/min from 700 to 800 °C. The air flow was maintained at 80 mL/min throughout the run. UV−vis (Shimazu UV-3600 plus) was used to collect the spectra of the suspension of reactant and flash products. XRD measurements were done by a Rigaku SmartLab Intelligent XRD system with filtered Cu Kα radiation (λ = 1.5406 Å). The scan rate was set as 1° per min.

ASSOCIATED CONTENT

Supporting Information

The Supporting Information is available free of charge at https://pubs.acs.org/doi/10.1021/acsnano.1c03536.

Safety instructions; TEM, SEM, and other images; XPS and Raman spectra; additional graphs (PDF)

AUTHOR INFORMATION

Corresponding Author

James M. Tour − *Department of Chemistry, Department of Materials Science and NanoEngineering, Smalley-Curl Institute, NanoCarbon Center, the Welch Institute for Advanced Materials, and Department of Computer Science, Rice University, Houston, Texas 77005, United States;* orcid.org/0000-0002-8479-9328; Email: tour@rice.edu

Authors

Weiyin Chen − *Department of Chemistry, Rice University, Houston, Texas 77005, United States*

John Tianci Li − *Department of Chemistry and Department of Materials Science and NanoEngineering, Rice University, Houston, Texas 77005, United States;* orcid.org/0000-0002-7218-8298

Zhe Wang − *Department of Chemistry, Rice University, Houston, Texas 77005, United States*

Wala A. Algozeeb − *Department of Chemistry, Rice University, Houston, Texas 77005, United States*

Duy Xuan Luong − *Department of Chemistry, Rice University, Houston, Texas 77005, United States;* orcid.org/0000-0001-7089-3359

Carter Kittrell − *Department of Chemistry, Rice University, Houston, Texas 77005, United States;* orcid.org/0000-0002-8449-4292
Emily A. McHugh − *Department of Chemistry, Rice University, Houston, Texas 77005, United States*
Paul A. Advincula − *Department of Chemistry, Rice University, Houston, Texas 77005, United States*
Kevin M. Wyss − *Department of Chemistry, Rice University, Houston, Texas 77005, United States*
Jacob L. Beckham − *Department of Chemistry, Rice University, Houston, Texas 77005, United States*
Michael G. Stanford − *Department of Chemistry, Rice University, Houston, Texas 77005, United States;* orcid.org/0000-0001-9663-1138
Bo Jiang − *Department of Chemistry, Rice University, Houston, Texas 77005, United States*

Complete contact information is available at:
https://pubs.acs.org/10.1021/acsnano.1c03536

Notes

The authors declare the following competing financial interest(s): Rice University owns intellectual property on the flash Joule heating strategy. J. M. T. and D. X. L. are or will be stockholders in Universal Matter LLC, the company that licensed the intellectual property from Rice University. Neither J. M. T. nor D. X. L. are officers or directors in the company. All conflicts of interest are managed through regular disclosure to the Rice University Office of Sponsored Programs and Research Compliance.

ACKNOWLEDGMENTS

The funding of the research is provided by the Air Force Office of Scientific Research (FA9550-19-1-0296) and the Department of Energy DOE-NETL (DE-FE0031794). The characterization equipment used in this project is from the Shared Equipment Authority (SEA) at Rice University. We thank Dr. Bo Chen for helpful discussion of the XPS results.

REFERENCES

(1) Gao, Y.; Cao, T.; Cellini, F.; Berger, C.; de Heer, W. A.; Tosatti, E.; Riedo, E.; Bongiorno, A. Ultrahard Carbon Film from Epitaxial Two-Layer Graphene. *Nat. Nanotechnol.* **2018**, *13*, 133−138.

(2) Ye, R.; Han, X.; Kosynkin, D. V.; Li, Y.; Zhang, C.; Jiang, B.; Marti, A. A.; Tour, J. M. Laser-Induced Conversion of Teflon into Fluorinated Nanodiamonds or Fluorinated Graphene. *ACS Nano* **2018**, *12*, 1083−1088.

(3) Sheka, E. F.; Golubev, Y. A.; Popova, N. A. Amorphous State of sp^2 Solid Carbon. *Fullerenes, Nanotubes, Carbon Nanostruct.* **2021**, *29*, 107−113.

(4) Toh, C. T.; Zhang, H.; Lin, J.; Mayorov, A. S.; Wang, Y. P.; Orofeo, C. M.; Ferry, D. B.; Andersen, H.; Kakenov, N.; Guo, Z.; Abidi, I. H.; Sims, H.; Suenaga, K.; Pantelides, S. T.; Ozyilmaz, B. Synthesis and Properties of Free-Standing Monolayer Amorphous Carbon. *Nature* **2020**, *577*, 199−203.

(5) Xu, D.; Chen, W.; Zeng, M.; Xue, H.; Chen, Y.; Sang, X.; Xiao, Y.; Zhang, T.; Unocic, R. R.; Xiao, K.; Fu, L. Crystal-Field Tuning of Photoluminescence in Two-Dimensional Materials with Embedded Lanthanide Ions. *Angew. Chem., Int. Ed.* **2018**, *57*, 755−759.

(6) Lin, J.; Peng, Z.; Liu, Y.; Ruiz-Zepeda, F.; Ye, R.; Samuel, E. L.; Yacaman, M. J.; Yakobson, B. I.; Tour, J. M. Laser-Induced Porous Graphene Films from Commercial Polymers. *Nat. Commun.* **2014**, *5*, 5714.

(7) Li, J. T.; Stanford, M. G.; Chen, W.; Presutti, S. E.; Tour, J. M. Laminated Laser-Induced Graphene Composites. *ACS Nano* **2020**, *14*, 7911−7919.

(8) Chen, M.; Pierstorff, E. D.; Lam, R.; Li, S. Y.; Huang, H.; Osawa, E.; Ho, D. Nanodiamond-Mediated Delivery of Water-Insoluble Therapeutics. *ACS Nano* **2009**, *3*, 2016−2022.

(9) Chen, W.; Wang, Z.; Bets, K. V.; Luong, D. X.; Ren, M.; Stanford, M. G.; McHugh, E. A.; Algozeeb, W. A.; Guo, H.; Gao, G.; Deng, B.; Chen, J.; Li, J. T.; Carsten, W. T.; Yakobson, B. I.; Tour, J. M. Millisecond Conversion of Metastable 2D Materials by Flash Joule Heating. *ACS Nano* **2021**, *15*, 1282−1290.

(10) Sun, Y.; Kvashnin, A. G.; Sorokin, P. B.; Yakobson, B. I.; Billups, W. E. Radiation-Induced Nucleation of Diamond from Amorphous Carbon: Effect of Hydrogen. *J. Phys. Chem. Lett.* **2014**, *5*, 1924−1928.

(11) Bagge-Hansen, M.; Bastea, S.; Hammons, J. A.; Nielsen, M. H.; Lauderbach, L. M.; Hodgin, R. L.; Pagoria, P.; May, C.; Aloni, S.; Jones, A.; Shaw, W. L.; Bukovsky, E. V.; Sinclair, N.; Gustavsen, R. L.; Watkins, E. B.; Jensen, B. J.; Dattelbaum, D. M.; Firestone, M. A.; Huber, R. C.; Ringstrand, B. S.; et al. Detonation Synthesis of Carbon Nano-Onions *via* Liquid Carbon Condensation. *Nat. Commun.* **2019**, *10*, 3819.

(12) Johnson, S. L.; Heimann, P. A.; MacPhee, A. G.; Lindenberg, A. M.; Monteiro, O. R.; Chang, Z.; Lee, R. W.; Falcone, R. W. Bonding in Liquid Carbon Studied by Time-Resolved X-Ray Absorption Spectroscopy. *Phys. Rev. Lett.* **2005**, *94*, 057407.

(13) Shenderova, O.; Koscheev, A.; Zaripov, N.; Petrov, I.; Skryabin, Y.; Detkov, P.; Turner, S.; Van Tendeloo, G. Surface Chemistry and Properties of Ozone-Purified Detonation Nanodiamonds. *J. Phys. Chem. C* **2011**, *115*, 9827−9837.

(14) Cebik, J.; McDonough, J. K.; Peerally, F.; Medrano, R.; Neitzel, I.; Gogotsi, Y.; Osswald, S. Raman Spectroscopy Study of the Nanodiamond-to-Carbon Onion Transformation. *Nanotechnology* **2013**, *24*, 205703.

(15) Kuznetsov, V. L.; Chuvilin, A. L.; Butenko, Y. V.; Mal'kov, I. Y.; Titov, V. M. Onion-Like Carbon from Ultra-Disperse Diamond. *Chem. Phys. Lett.* **1994**, *222*, 343−348.

(16) Su, Z.; Zhou, W.; Zhang, Y. New Insight into the Soot Nanoparticles in a Candle Flame. *Chem. Commun.* **2011**, *47*, 4700−4702.

(17) Kumar, A.; Ann Lin, P.; Xue, A.; Hao, B.; Khin Yap, Y.; Sankaran, R. M. Formation of Nanodiamonds at Near-Ambient Conditions *via* Microplasma Dissociation of Ethanol Vapour. *Nat. Commun.* **2013**, *4*, 2618.

(18) Bakharev, P. V.; Huang, M.; Saxena, M.; Lee, S. W.; Joo, S. H.; Park, S. O.; Dong, J.; Camacho-Mojica, D. C.; Jin, S.; Kwon, Y.; Biswal, M.; Ding, F.; Kwak, S. K.; Lee, Z.; Ruoff, R. S. Chemically Induced Transformation of Chemical Vapour Deposition Grown Bilayer Graphene into Fluorinated Single-Layer Diamond. *Nat. Nanotechnol.* **2020**, *15*, 59−66.

(19) Chen, W.; Salvatierra, R. V.; Ren, M.; Chen, J.; Stanford, M. G.; Tour, J. M. Laser-Induced Silicon Oxide for Anode-Free Lithium Metal Batteries. *Adv. Mater.* **2020**, *32*, 2002850.

(20) Ye, R.; Chyan, Y.; Zhang, J.; Li, Y.; Han, X.; Kittrell, C.; Tour, J. M. Laser-Induced Graphene Formation on Wood. *Adv. Mater.* **2017**, *29*, 1702211.

(21) Chyan, Y.; Ye, R.; Li, Y.; Singh, S. P.; Arnusch, C. J.; Tour, J. M. Laser-Induced Graphene by Multiple Lasing: Toward Electronics on Cloth, Paper, and Food. *ACS Nano* **2018**, *12*, 2176−2183.

(22) Luong, D. X.; Bets, K. V.; Algozeeb, W. A.; Stanford, M. G.; Kittrell, C.; Chen, W.; Salvatierra, R. V.; Ren, M.; McHugh, E. A.; Advincula, P. A.; Wang, Z.; Bhatt, M.; Guo, H.; Mancevski, V.; Shahsavari, R.; Yakobson, B. I.; Tour, J. M. Gram-Scale Bottom-Up Flash Graphene Synthesis. *Nature* **2020**, *577*, 647−651.

(23) Yao, Y.; Huang, Z.; Xie, P.; Lacey, S. D.; Jacob, R. J.; Xie, H.; Chen, F.; Nie, A.; Pu, T.; Rehwoldt, M.; Yu, D.; Zachariah, M. R.; Wang, C.; Shahbazian-Yassar, R.; Li, J.; Hu, L. Carbothermal Shock Synthesis of High-Entropy-Alloy Nanoparticles. *Science* **2018**, *359*, 1489−1494.

(24) Wang, C.; Ping, W.; Bai, Q.; Cui, H.; Hensleigh, R.; Wang, R.; Brozena, A. H.; Xu, Z.; Dai, J.; Pei, Y.; Zheng, C.; Pastel, G.; Gao, J.; Wang, X.; Wang, H.; Zhao, J.-C.; Yang, B.; Zheng, X.; Luo, J.; Mo, Y.;

et al. A General Method to Synthesize and Sinter Bulk Ceramics in Seconds. *Science* **2020**, *368*, 521−526.

(25) Yao, Y.; Huang, Z.; Xie, P.; Wu, L.; Ma, L.; Li, T.; Pang, Z.; Jiao, M.; Liang, Z.; Gao, J.; He, Y.; Kline, D. J.; Zachariah, M. R.; Wang, C.; Lu, J.; Wu, T.; Li, T.; Wang, C.; Shahbazian-Yassar, R.; Hu, L. High Temperature Shockwave Stabilized Single Atoms. *Nat. Nanotechnol.* **2019**, *14*, 851−857.

(26) Stanford, M. G.; Bets, K. V.; Luong, D. X.; Advincula, P. A.; Chen, W.; Li, J. T.; Wang, Z.; McHugh, E. A.; Algozeeb, W. A.; Yakobson, B. I.; Tour, J. M. Flash Graphene Morphologies. *ACS Nano* **2020**, *14*, 13691−13699.

(27) Dou, S.; Xu, J.; Cui, X.; Liu, W.; Zhang, Z.; Deng, Y.; Hu, W.; Chen, Y. High-Temperature Shock Enabled Nanomanufacturing for Energy-Related Applications. *Adv. Energy Mater.* **2020**, *10*, 2001331.

(28) Gogotsi, Y.; Welz, S.; Ersoy, D. A.; McNallan, M. J. Conversion of Silicon Carbide to Crystalline Diamond-Structured Carbon at Ambient Pressure. *Nature* **2001**, *411*, 283−287.

(29) Xiao, J.; Li, J. L.; Liu, P.; Yang, G. W. A New Phase Transformation Path from Nanodiamond to New-Diamond *via* an Intermediate Carbon Onion. *Nanoscale* **2014**, *6*, 15098−15106.

(30) Algozeeb, W. A.; Savas, P. E.; Luong, D. X.; Chen, W.; Kittrell, C.; Bhat, M.; Shahsavari, R.; Tour, J. M. Flash Graphene from Plastic Waste. *ACS Nano* **2020**, *14*, 15595−15604.

(31) Kamali, A. R.; Fray, D. J. Preparation of Nanodiamonds from Carbon Nanoparticles at Atmospheric Pressure. *Chem. Commun.* **2015**, *51*, 5594−5597.

(32) Ferrari, A. C.; Robertson, J. Raman Spectroscopy of Amorphous, Nanostructured, Diamond-Like Carbon, and Nanodiamond. *Philos. Trans. R. Soc., A* **2004**, *362*, 2477−2512.

(33) Prawer, S.; Nemanich, R. J. Raman Spectroscopy of Diamond and Doped Diamond. *Philos. Trans. R. Soc., A* **2004**, *362*, 2537−2565.

(34) Obraztsova, E. D.; Fujii, M.; Hayashi, S.; Kuznetsov, V. L.; Butenko, Y. V.; Chuvilin, A. L. Raman Identification of Onion-Like Carbon. *Carbon* **1998**, *36*, 821−826.

(35) Wu, G.; McHugh, E. A.; Berka, V.; Chen, W.; Wang, Z.; Beckham, J. L.; Derry, P. J.; Roy, T.; Kent, T. A.; Tour, J. M.; Tsai, A. L. Oxidized Activated Charcoal Nanoparticles as Catalytic Superoxide Dismutase Mimetics: Evidence for Direct Participation of an Intrinsic Radical. *ACS Appl. Nano Mater.* **2020**, *3*, 6962−6971.

(36) Araujo, P. T.; Terrones, M.; Dresselhaus, M. S. Defects and Impurities in Graphene-Like Materials. *Mater. Today* **2012**, *15*, 98−109.

(37) Osswald, S.; Yushin, G.; Mochalin, V.; Kucheyev, S. O.; Gogotsi, Y. Control of sp^2/sp^3 Carbon Ratio and Surface Chemistry of Nanodiamond Powders by Selective Oxidation in Air. *J. Am. Chem. Soc.* **2006**, *128*, 11635−11642.

(38) Ohm, M.; Gravenstein, N.; Good, M. L. Duration of Carbon Dioxide Absorption by Soda Lime at Low Rates of Fresh Gas Flow. *J. Clin. Anesth.* **1991**, *3*, 104−107.